Available online at www.sciencedirect.com

ScienceDirect

journal homepage: www.elsevier.com/locate/he

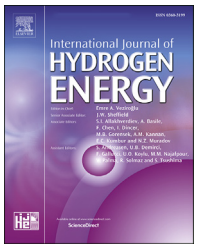

Impact of H_2-enriched natural gas on pollutant emissions from domestic condensing boilers: numerical simulations of the combustion chamber

Rachele Lamioni [a,*], *Cristiana Bronzoni* [b], *Marco Folli* [b], *Leonardo Tognotti* [a], *Chiara Galletti* [a]

[a] *Dipartimento di Ingegneria Civile e Industriale, Università di Pisa, 56126 Pisa, Italy*
[b] *Ricerca & Sviluppo - Laboratorio Sviluppo Prodotti, Immergas S.p.A., Brescello (RE), Italy*

HIGHLIGHTS

- Simulations with detailed kinetics of the combustion chamber in a condensing boiler.
- Conjugate Heat Transfer to model the coil.
- Interaction of premixed flames from neighbor holes and slits of the burner.
- Successful validation of the model against measurements of CO and NO emissions.
- Adding hydrogen has a beneficial effect on both CO and NO emissions.

ARTICLE INFO

Article history:
Received 26 September 2022
Received in revised form
16 January 2023
Accepted 8 February 2023
Available online 25 February 2023

Keywords:
Laminar premixed flame
Green energy vectors
Hydrogen
Perforated burner
Computational Fluid Dynamics
Heat exchange

ABSTRACT

The addition of green hydrogen to the gas mixture feeding domestic boilers may help the ecological transition of the residential sector. However, there are concerns about the combustion process as hydrogen shows power density and reactivity that are much different than those of natural gas. In this work, we perform three-dimensional simulations with detailed kinetics to describe and comprehend the combustion process in a real modern boiler, equipped with a perforated premixed burner (presenting a pattern of small holes and slits), with the purpose also to evaluate the impact of green hydrogen. The flame structure is complex and characterized by the interaction of flames exiting from neighbor holes and slits; these flames may merge and lead to very intense flames, especially at high flow rates. The presence of a flow distributor, upstream of the burner, induces different velocities at the holes and slits, ultimately affecting the morphology, propagation and interactions of the flames. This behavior is observed for all investigated H_2 concentrations, i.e., up to 50% by vol. The model is validated against available measurements of carbon monoxide and nitric oxides in flue gases, which both indicate very satisfactory predictions. More specifically, the addition of green H_2 has a beneficial effect on both CO and NO emissions. More specifically the CO emissions at the nominal power are observed to diminish from 154 to 18 ppm when shifting from 0 to 50% H_2 in the fuel mixture, while NO emissions decrease from 20 to only 5 ppm. This latter reduction is a surprising and encouraging result; the reason is due to the fact that the addition of hydrogen in the fuel mixture leads naturally to more dilute operating conditions in a condensing boiler. We

* *Corresponding author.*
E-mail address: rachele.lamioni@unipi.it (R. Lamioni).
https://doi.org/10.1016/j.ijhydene.2023.02.040

believe that the proposed model represents a valid tool to explore strategies to improve the combustion process with alternative fuels.

Introduction

The European Commission recently presented *Fit for* 55 program, a roadmap with specific actions and targets until 2030 to achieve a climate-neutral and resource-conserving Europe by 2050 as declared in the EU Green Deal. More specifically, the *Fit for* 55 program plans a 55% reduction in CO_2 emissions by 2030, compared to those in 1990 [1], thus asking for an urgent increase of the share of renewables. This is also extremely important to diversify our energy mix, to improve the resilience of our energetic system by reducing our dependence on suppliers of fossil fuels ("REPowerEU" action [2]).

In Europe, the residential sector accounts for approximately 30% of final energy consumption, and to fulfill the above environmental targets, it is well accepted that at least two-thirds of this energy should be provided by electricity by 2050. However, this goal requires expensive upgrade of our heating infrastructure, which is actually rather obsolete [3,4]. Gas boilers are the main heating devices, being for instance installed in more than 85% and 90% of homes in the UK and the Netherlands, respectively [5]. Recently International Energy Agency, recommends that only zero carbon-ready gas boilers, i.e., compatible with hydrogen, can be sold after 2023 [6,7].

Indeed green hydrogen, produced by water electrolysis from excess wind and solar power [8], can strongly help the decarbonization of residential heating by providing an energy vector to be burn in gas boilers [9,10]. Hydrogen benefits from the potential of retrofitting the existing natural gas grid for storage and distribution, even though this transformation to deal with 100% H_2 would require substantial efforts and take place gradually [11–15], highlighting the need for innovative solutions [16]. However, there are very encouraging demonstration of hydrogen addition into the existing gas network up to 20% [12,17–20].

Modern condensing boilers are equipped with perforated burners injecting a premixed mixture into the combustion chamber. So far, the burner design is based on the manufacturers' experience [21]; however, the upcoming changes in gas composition, with the introduction of hydrogen would require a better understanding of the combustion process, to better optimize the burner and the flame detector, which should be specifically designed for each fuel. Indeed hydrogen shows reactivity and power density differing significantly from those of natural gas. For instance the adiabatic flame temperature is approximately $T_{ad} = 2380$K, thus much higher than that of methane, i.e., $T_{ad} = 2220$K, and this may lead to adverse effects on formation of nitric oxides, whose thermal formation pathways is strongly enhanced at high temperatures. Even more dramatic is the change in the flame speed, which is $S_L = 2.7$ m/s for hydrogen, thus about eight times larger than that of methane, i.e., $S_L = 0.35$ m/s. These differences asks for a better comprehension of the combustion physics inside domestic condensing boilers to well deal with green fuels by ensuring efficient and safe conversion with a low impact on the environment [22].

In this context, the application of mathematical models based on computational fluid dynamics (CFD) which is able to provide us with a large details of information, is partially hampered by the complexity of premixed flames, as well as by the computational cost required to describe transport, reaction, and heat exchange in complex domains.

Indeed, only a few numerical simulations of burners in domestic boilers can be found, and most of them are limited to the mixing problem or to simplified computational domains. As an example, Zhao et al. [23] carried out non-reactive CFD simulations to estimate the influence of the geometry on the gas distribution from a perforated cylindrical burner, while Zhang et al. [24] used CFD to optimize the gas mixing system upstream of the burner.

Altay et al. [25] performed 2-dimensional numerical simulations of laminar premixed methane-air flames from a single hole of a flat perforated multi-hole burner and observed that the flame morphology strongly depends on the heat exchange between the flame and the burner plate. Kedia and Ghoniem [26] carried out 2-dimensional simulations to investigate the stabilization mechanism of a laminar methane-air premixed flame issuing from a multi-hole burner. Jithin et al. [27] showed through 3-dimensional simulations of premixed propane-air flames from a flat perforated burner that the flame stand-off distance increases with the thermal conductivity of the burner plate. Numerical simulations were employed by Veetil et al. [28] to analyse how the pattern and hole-to-hole distance affect the flames from a flat perforated plate. Detailed kinetics was used by Lamioni et al. [29] to investigate the effect of the hole-to-hole distance on the flame structure of premixed laminar flames from a multi-hole burner fed with H_2-enriched natural gas. Simulations showed how the addition of hydrogen leads to an anticipation of the flame front. Detailed kinetics was used by Lamioni et al. [29,30] to investigate the effect H_2 addition on the structure of premixed flames issuing from multi-hole and multi-slit burners. Simulations showed how the addition of hydrogen leads to an anticipation of the flame front. Besides, different and complex flame morphologies were observed for different thermal loads.

Hassan et al. [31] developed a 2D CFD model of the combustion chamber of a domestic condensing boiler equipped with a cylindrical multi-hole burner. The domain consists on a slice of the chamber. The authors showed a decrease of CO emissions when reducing the inlet velocity in accordance with experimental data, even though the CFD model significantly

over-predicted the CO values. This behavior was imputed to the fact that the model does not take into account the heat exchanges and thus neglects the residence time there.

Hinrichs et al. [32] developed a 3-dimensional model with detailed chemistry of a premixed methane-air flame from single hole in a perforated cylindrical burner. The authors included in the domain a region emulating the heat exchange, and showed how the CO concentration depends strongly on the fuel gas cooling. Indeed, the amount of CO in the flue gases was significantly higher than the chemical equilibrium one that should be nearly zero at the outlet temperature. Indeed, as the flue gases cross the heat exchanger, the CO oxidization reactions to CO_2 are hampered as the radical concentrations quickly drop. Very recently the same research group [33] developed a CFD model of the entire combustion chamber of a domestic condensing boiler by treating the chemistry with the flamelet progress variable. The multi-hole cylindrical burner was modeled as a porous medium while the cooling coils were included in the computations through the Conjugate Heat Transfer approach. Results highlighted the complexity of the flow-field and flame structures, due to locally varying burner outflow velocities. The model provided reasonable predictions of pollutants: the CO emissions were underestimated by 47%, while NOx emissions were over-predicted by 18%.

In this work, we develop a 3-dimensional CFD model with resolved kinetics of the combustion chamber of a domestic condensing boiler. The boiler is equipped with a perforated cylindrical burner presenting a pattern of small holes and slits that inject a premixed gas consisting of H_2-enriched natural gas and air. The model is applied to different cases spanning different thermal loads and H_2 contents in the gas mixtures up to 50% by vol. and validated against experimental measurements of pollutant emissions, i.e., of carbon monoxide and nitrogen oxides. Hence, our ultimate goal is to provide a tool to be used for the burner design to ensure the efficient use of green energy vectors for decarbonizing domestic heating, while also limiting other pollutants such as nitric oxides.

Test case and operating conditions

The domestic condensing boiler under investigation has a nominal power of 25 kW and is manufactured by Immergas S.p.A. The boiler is equipped with a perforated cylindrical burner with an inner diameter of 60 mm (see Fig. 1a) from Polidoro S.p.A [34], and a stainless steel coil condensing unit (Fig. 1) from Condevo S.p.A [35]. The burner injects the premixed fuel-air mixture thanks to a pattern of small holes and slits, generating short-length flames that accommodate the compact volume of the chamber within the coil.

In the test rig, the boiler is fed with natural gas, i.e., G20 test gas, and two H_2-admixtures, i.e., G222 and H2NG gases, whose H_2 content is 23% and 50% by volume, respectively, as reported in Table 1. For the G20 test gas, a run was also performed using a minimum power, i.e., 4 kW.

The nominal thermal power of 25 kW holds for the reference case with natural gas (G20). In this case the optimal equivalence ratio is $\varphi = 0.8$ [36]. The addition of H_2 in the gas mixture causes a change in both the thermal power and the equivalence ratio as explained in Ref. [37] and also applied in Ref. [29].

Indeed, at constant supply pressure, the fuel volumetric flow rate F changes with composition, and hence, with density as

$$F \propto \frac{1}{\sqrt{\rho/\rho_0}} \tag{1}$$

with ρ_0 being the density of air at 0°C. This behavior causes a change in the thermal power which ultimately results to be proportional to the Wobbe index W as:

$$P_{th} = F \cdot HHV \propto \frac{HHV}{\sqrt{\rho/\rho_0}} \propto W \tag{2}$$

The estimated Wobbe indexes (at 25°C) and thermal powers for the three investigated gas mixtures are listed in Table 1.

The equivalence ratio can be expressed as a function of the stoichiometric air requirement, i.e., LdV, which is the volume of air required to oxidize one volume of fuel [37], as:

$$\varphi = \frac{(F/A)}{(F/A)_{st}} = (F/A) \cdot Ldv \tag{3}$$

where F and A are the volumetric flow rates of the fuel and air, respectively, while the subscript st denotes the stoichiometric conditions.

At constant supply pressure, the pressure of the fuel entering the burner does not depend on composition and therefore the momentum of the fuel jet is constant. In this conditions the air flow rate, i.e., A, will also be constant, in burners having a Venturi to draw air [37]. The replacement of the G20 gas with H_2-admixtures, leads to smaller equivalence ratios according to the following relationship [37]:

$$\Delta\varphi = \varphi_{H2adm} - \varphi_{G20} = \varphi_{G20}\left[\frac{Ldv_{G20}}{Ldv_{H2adm}} \cdot \sqrt{\frac{\rho_{G20}}{\rho_{H2adm}}} - 1\right] \tag{4}$$

The estimated equivalence ratios for the H_2-admixtures are reported in Table 1.

The positive effect on decarbonization, resulting from the substitution of part of methane with a non-carbon fuel, is provided in the last column of Table 1. The percentage reduction in CO_2 is estimated here by normalizing it to the same thermal input (as P_{th} changes for different H_2 contents). We notice how the use of 23% of hydrogen in the fuel mixture leads to an 8.7% cut of CO_2 emissions, while 50% of hydrogen ensures a CO_2 reduction of 24.2% with respect to methane, i.e., G20 test gas. For each experimental condition, pollutant emissions in terms of CO and CO_2 are measured using Carbon dioxide analyzer (Siemens ULTRAMAT 7), while NOx are measured using a single-channel multi-gas analyzer (nCLD 63, Eco Physics AG, Dürnen, Switzerland).

Numerical model

Computational domain

The computational domain of the entire chamber is rather complex as there are aspects that cannot be neglected or

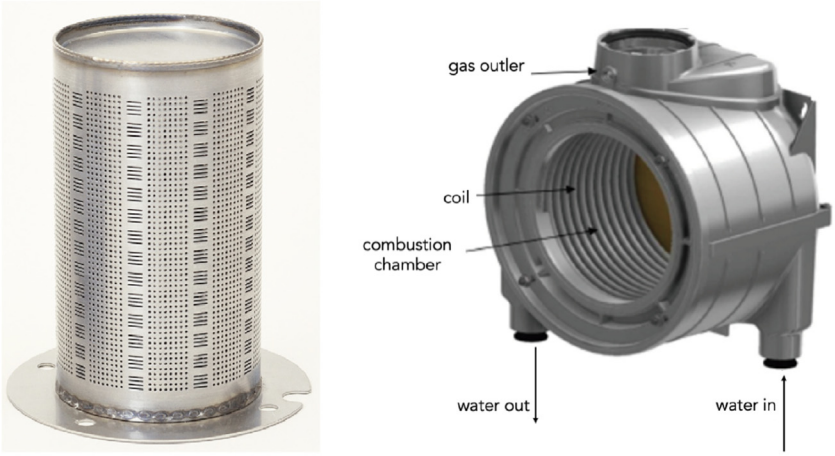

Fig. 1 – Picture of (a) the burner (courtesy of Polidoro S.p.A) and (b) the heat exchanger (courtesy of Condevo S.p.A.).

simplified if we want to well reproduce its real behavior. Indeed, as described above, the burner shows a pattern of small holes and slits: more specifically there are more than 2000 of them. We should be able to model every single flame which means that we should resolve its flame front. Luckily, we can exploit the burner symmetry and restrict our domain to just a 20° wedge. Besides, the burner is equipped internally with a cylindrical distributor, which also presents a series of holes. Actually, the presence of the distributor may affect the gas velocity in each hole and slit of the burner and ultimately the morphology of the flames; so the distributor should be considered in the model to make it more faithful to reality. However, since reactions do not occur upstream of the burner, we can carry out non-reactive simulations there to reduce the computational cost. Indeed, these non-reactive simulations allow estimating the velocity in the holes and slits to feed the reactive model of the combustion chamber. More specifically, a 20° wedge is also considered for the distributor model. Finally, since we are interested also in estimating CO emissions, which greatly depend on the quenching of CO oxidation reactions [32] due to the flue gas cooling, the heat exchanger has to be included in the domain. For this purpose, we employ the Conjugate Heat Transfer in which the heat transfer is solved in both fluid and solid domains. In this manner we overcome the problem of setting unknown boundary conditions at the wall of the coils, as this boundary is required when modeling just the fluid zone. Practically, the coil is treated as a solid domain with a heat sink. The amount of heat that is removed is estimated from the operating conditions, taking into account that we are modeling a 20° wedge. More specifically, the sink of heat is estimated just dividing the actual power by the volume of the coils.

Table 1 – Composition of the test gases, corresponding Wobbe index, thermal power, equivalence ratio and CO_2 reduction per unit power for the investigated runs.

Test gas	H_2	CH_4	W	P_{th}	φ	CO_2 reduction
	[% by vol]	[% by vol]	[–]	[kW]	[–]	[%]
G20	0	100	53.5	4	0.8	0
G20	0	100	53.5	25	0.8	0
G222	23	77	50.5	23.6	0.74	8.7
H2NG	50	50	47.0	22.0	0.67	24.2

An overview of the whole computational domain is given in Fig. 2a. Please note that the non-reactive simulations of the flow distributor are performed separately and obtained results feed to the reactive simulations involving the combustion chamber, the heat exchanger and the outlet region. For sake of clarity, the distributor region is depicted in Fig. 2b. Here we can notice the two semi-rows of holes of the flow distributor upstream of the holes and slits of the burner.

As for the computational grid, 400k polyhedral cells (Fig. 3b) are needed, according to a preliminary grid independence study (carried out with a number of polyhedral cells ranging from 200k to 1.2 M) for the flow distributor region. The combustion chamber alone requires a polyhedral grid made of 4.6 M polyhedral cells. In addition to the grid independence study, preliminary 1D simulations of freely propagating laminar premixed flames are carried out by using Cantera [38] to determine the flame front thickness and hence the required cell size to well describe the combustion process [29]. The remainder of the domain, i.e. outlet region and heat exchanger, is also meshed with a polyhedral grid. The overall grid including the combustion chamber one, is shown in Fig. 3a, and contains approximately 6.0 M cells.

Physical model

The regime is laminar with typical Reynolds numbers $Re < 50$, as holes and slits are very small. The problem can be described by the Navier-Stokes, energy and transport/reaction equations for chemical species. As mentioned before, in the distributor model, only the former equations are solved. Since

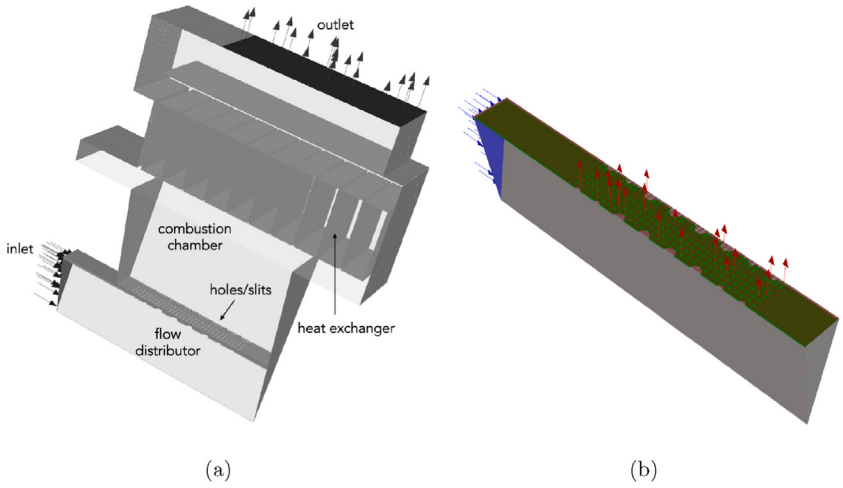

Fig. 2 – (a) Entire computational domain and (b) flow distributor domain.

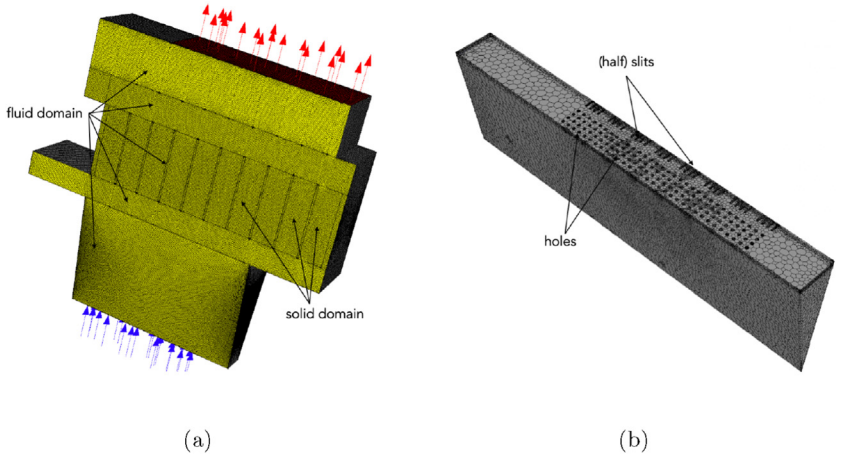

Fig. 3 – Computational grid for (a) combustion chamber and heat exchanger and (b) for the flow distributor.

we do not expect instabilities for the present operating conditions and hole/slit dimensions, these equations can be written and solved in the steady-state form as:

$$\nabla\cdot(\rho\mathbf{v}) = 0 \tag{5}$$

$$\nabla\cdot(\rho\mathbf{v}\mathbf{v}) = \nabla p + \nabla\cdot(\bar{\boldsymbol{\tau}}) \tag{6}$$

$$\nabla\cdot(\mathbf{v}(\rho E + p)) = \nabla\cdot(k\nabla T) + S_h \tag{7}$$

$$(\rho Y_i) + \nabla\cdot(\rho\mathbf{v}Y_i) = -\rho\mathcal{D}_i\nabla^2 Y_i + R_i \tag{8}$$

where $\mathbf{v}$ is velocity, $\bar{\boldsymbol{\tau}}$ is the stress tensor, S_h is the energy source term, including the contribution of radiation, Y_i is the mass fraction of the i-th chemical species and k is the effective thermal conductivity. R_i is the net rate of production or destruction of the i-th chemical species by chemical reaction. $\mathcal{D}_i$ is the molecular diffusion coefficient of the i-th chemical species in the mixture. Binary diffusion coefficients are firstly calculated following the kinetic theory and a modification of the Chapman–Enskog formula; then $\mathcal{D}_i$ is obtained by applying Wilke's mixing rule. The kinetic mechanism is KEE-58 [39] oxidation scheme, which consists of 17 chemical species and 58 reversible reactions. This choice is verified by performing preliminary simulations on a smaller portion of the domain with the complete GRI3.0 scheme, showing good agreement. In particular, these results are shown in Appendix A.

Radiation is taken into account with the P1 model [40,41] using the weighted-sum-of-gray-gases model with coefficients from Smith [42] to estimate the spectral properties of the gas media. Emissions of nitric oxides are estimated by including the thermal, prompt, N_2O and NNH-intermediate pathways. The thermal formation is modeled from the Zeldovich scheme by assuming a steady-state for the N radical [43], while the O radical are available in the KEE-Mech scheme. The prompt NO formation from methane is estimated from the one-step mechanism proposed by De Soete [44], while the N_2O intermediate from the 2-step scheme of [45] by assuming a steady state for N_2O. As for the NNH route, the mechanism of Konnov [46] is implemented in the code through a bespoke subroutine as explained in Refs. [47,48].

Boundary conditions

An uniform velocity is set at the entrance to the flow distributor. The velocity value is estimated in the range of the experimental powers, i.e., 4 and 25 kW. Subsequently, as explained before, the predicted velocity profiles in the holes and slits are given to the reactive flow simulations. As for the solid domain corresponding to the heat exchanger, an heat sink per volume is imposed. The value is obtained by dividing the power to the total volume of the coil. Symmetry conditions are given to the lateral walls of the domain while a pressure outlet condition is imposed to the outlet.

Solution methodology

The above set of equations with related boundary conditions is solved with the pressure-based coupled algorithm available in the finite volume code FLUENT 19.2 [43] by ANSYS Inc., using a central differencing scheme for diffusion terms and second-order upwind scheme for convection terms. The computation of the chemistry is carried out through the direct integration method. The fuel-oxidizer mixture is ignited by patching a region near the inlet with a temperature higher than the adiabatic one, i.e. with $T = 2500$ K. At convergence, normalized residuals do not change with iterations and are all below 10^{-6}.

Results

Effect of flow distributor

As mentioned above, a preliminary analysis is carried out to determine the effective flow velocity at each hole and slit to

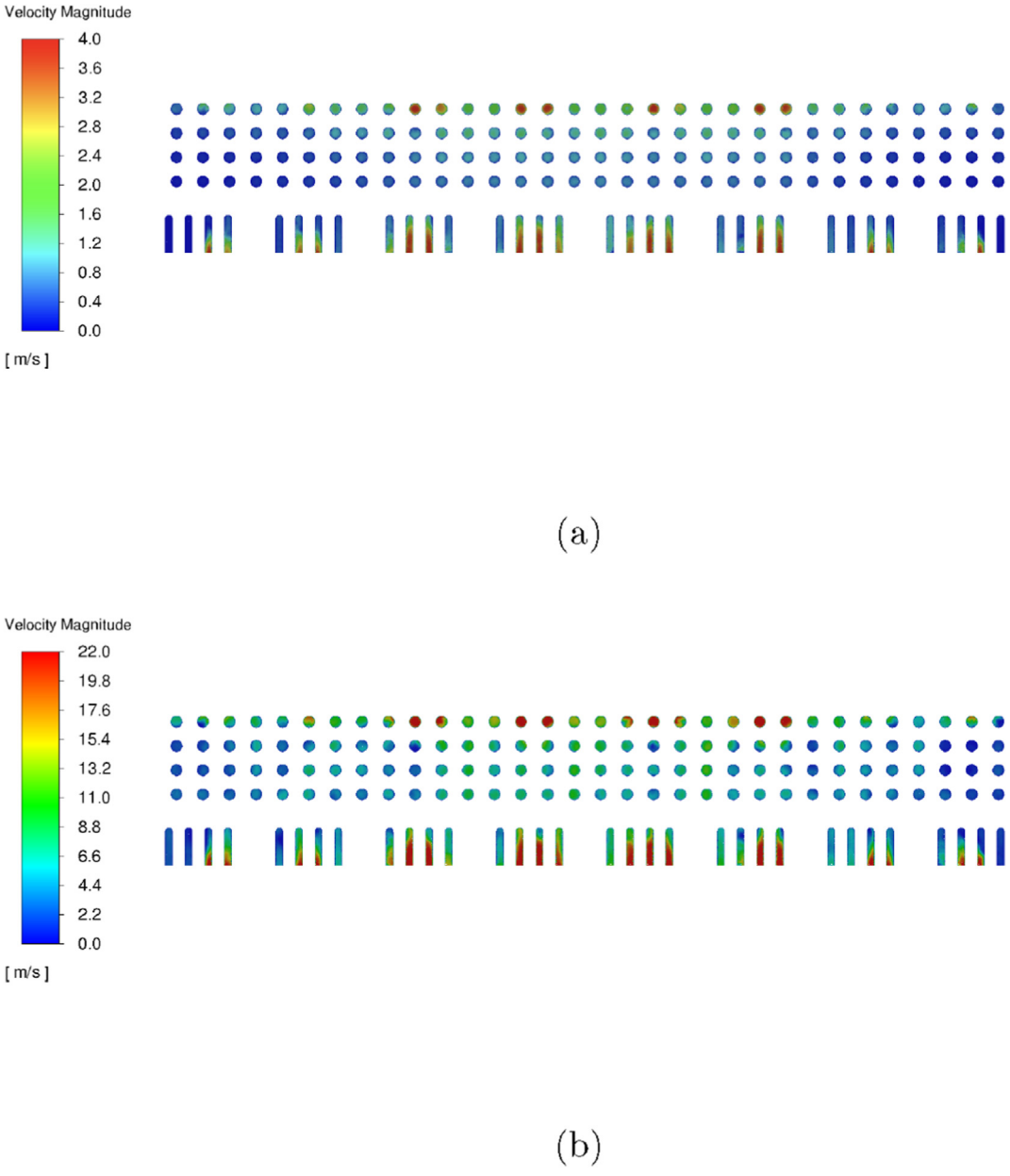

Fig. 4 – Velocity field at the burner entrance predicted for: (a) the minimum power (4 kW) and (b) the nominal power (25 kW).

fed the CFD model of the chamber. In this analysis, non-reactive simulations are carried out. Results are shown in Fig. 4 for the minimum and maximum thermal load. We observe for both conditions that the flow field is not uniform, with some holes being more fed than others. The same occurs for the slits. Besides, some slits show velocity gradients. Hence we may expect a complex behavior, that is different from what one would expect by feeding uniformly the burner.

Effect of thermal load

Fig. 5 shows the temperature field for a plane passing through a row of holes and a row of slits for the minimum power, i.e., 4 kW, when feeding natural gas, i.e, G20 test gas. Although the CFD simulations cover the combustion chamber and the heat exchanger regions, the fields shown here refer only to the near burner region fro the sake of clarity. Similarly, Fig. 6 reports the distribution of OH, a well-known marker, to appreciate the structure of the flames issuing from the groups of holes and slits. We can notice how the morphology of the flames in the region of holes (Fig. 5a) is much different than the one in the region of slits (Fig. 5b). Indeed a flat flame occurs from the holes, even though a slightly higher OH distribution is noticed in the central region of the burner. Conversely, the flames from the slits appear more intense. Besides, the different local velocity, due to the presence of the distributor upstream of the burner, promotes the merging of flames issuing from neighbor slits, leading to rather big flames. Finally, we can also observe that flames are not produced in the group of slits at the edge of the burner located on the opposite side to the gas entrance.

Even though the combustion chamber is not accessible for measurements, some images in the open air are available from the burner supplier, i.e., Polidoro S.p.A [34]. The image for the minimum load, i.e., 4 kW, is reported in Fig. 7a. Although such images should be considered only as indicators of qualitative behavior, as they refer to open air, i.e. without the confinement due to the chamber, we can notice the merging of the flames from the groups of slits. Considering one of the areas characterized by the groups of slits (white box), we notice the merge of the flames generated by the slits. In addition, flames appear less intense near the edge of the burner, as also we can deduce from the OH fields of Fig. 6.

With increasing the power to the nominal value, i.e., 25 kW shown in Fig. 8, we observe a modification of the flame

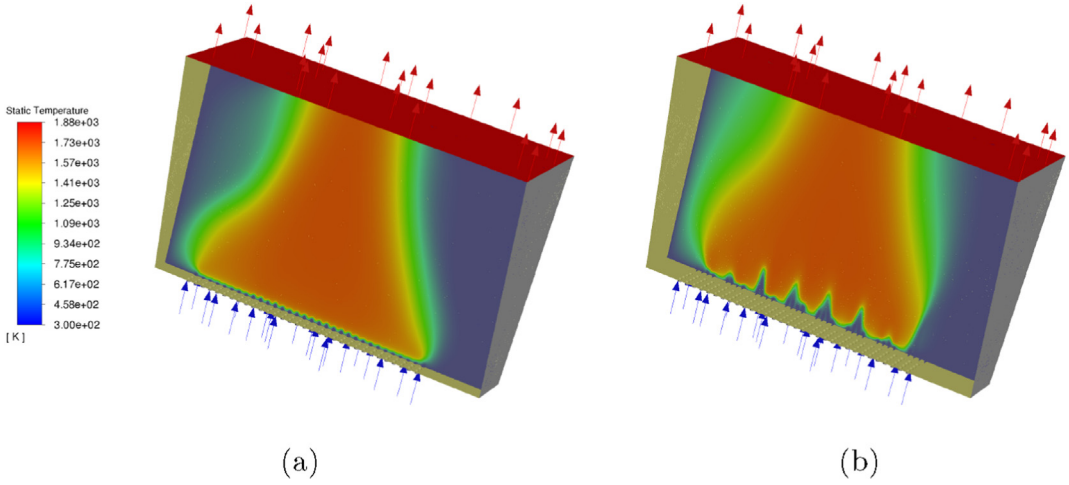

Fig. 5 – Temperature field on the (a) holes and (b) slits for the minimum power (4 kW).

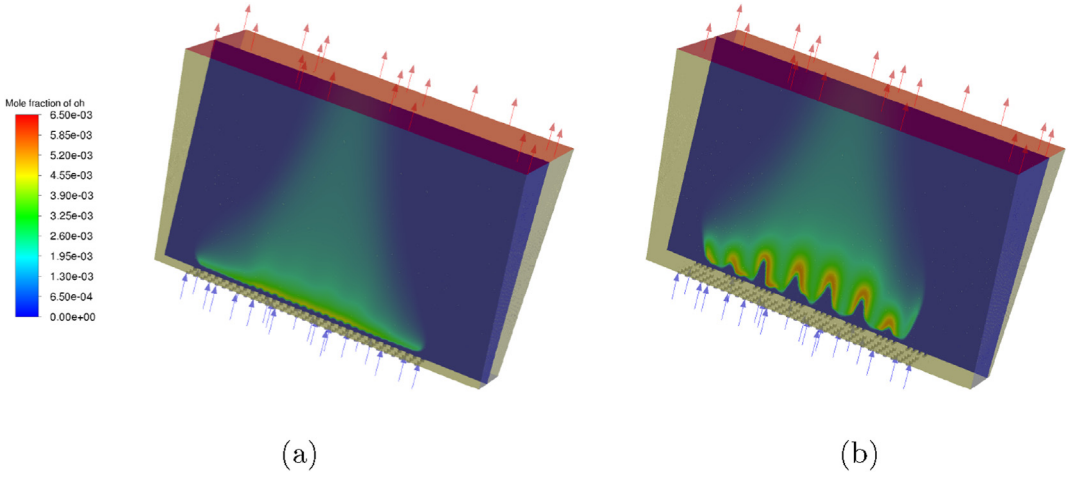

Fig. 6 – OH field for a plane passing through a row of (a) holes and (b) slits for the nominal power (4 kW).

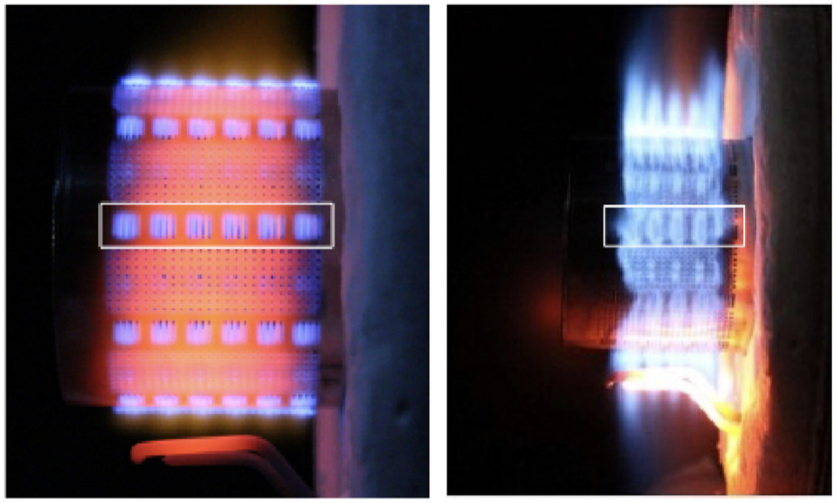

(a) (b)

Fig. 7 – Images taken in open air for: (a) the minimum power (4 kW) and (b) the nominal power (25 kW). Courtesy of Polidoro S.p.A.

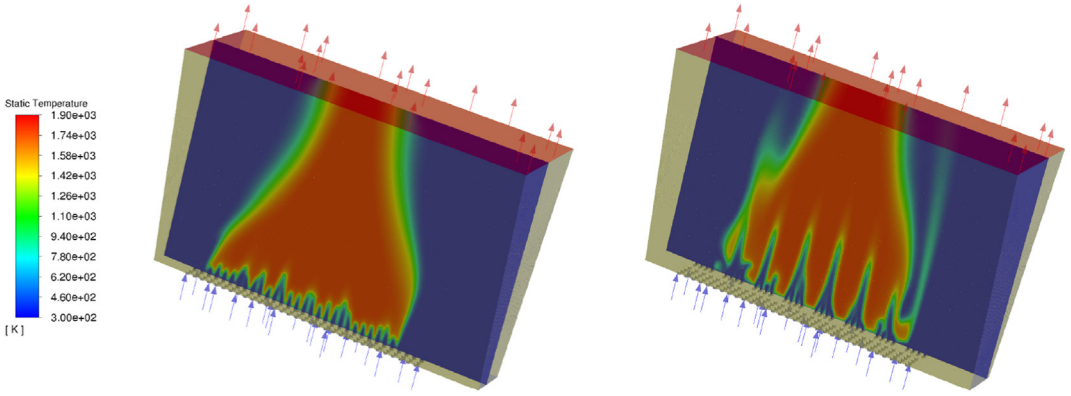

(a) (b)

Fig. 8 – Temperature field for a plane passing through a row of (a) holes and (b) slits for the nominal power (25 kW).

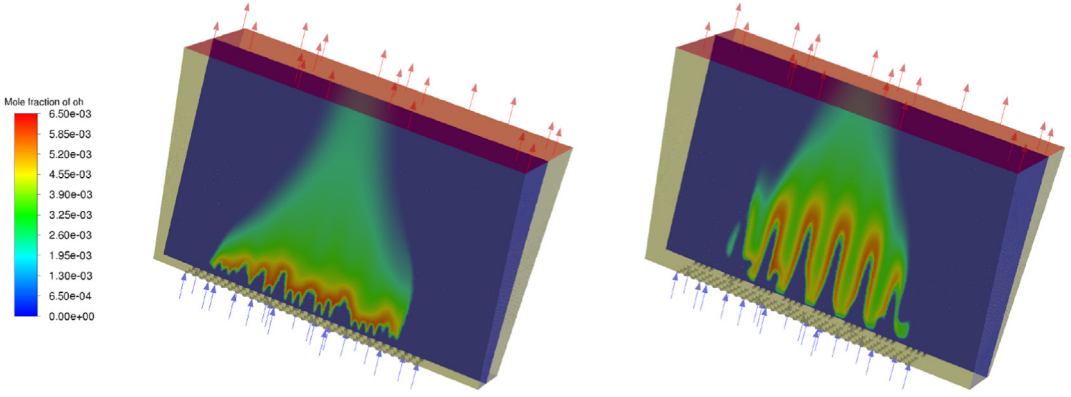

(a) (b)

Fig. 9 – OH field for a plane passing through a row of holes (a) and slits (b) for the nominal power (25 kW).

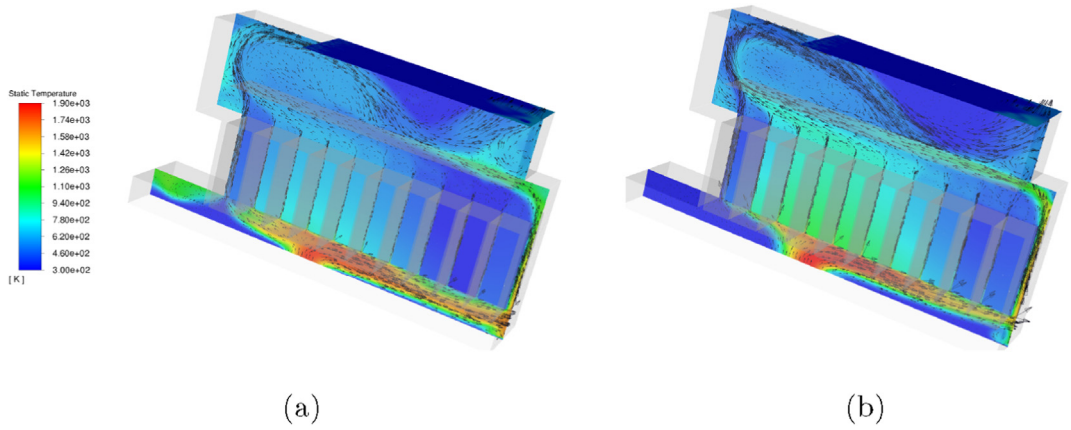

Fig. 10 – Temperature field at the heat exchanger region for the (a) the minimun (4 kW) and (b) the nominal power (25 kW).

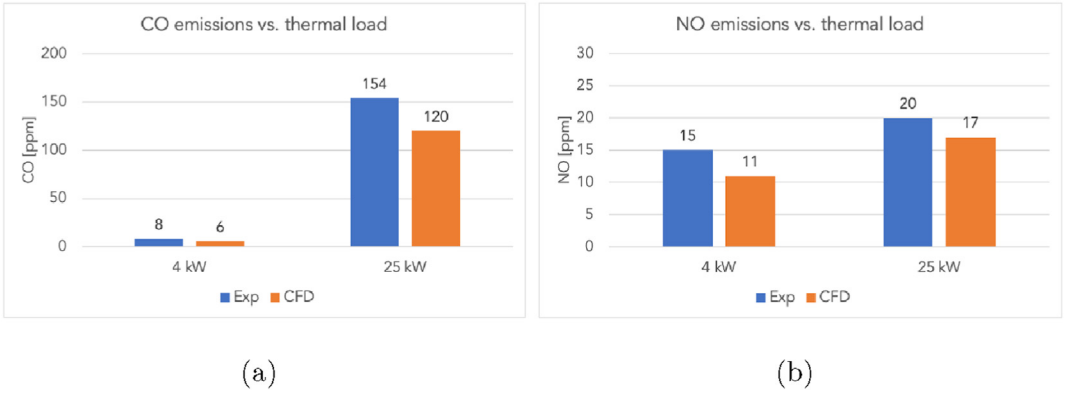

Fig. 11 – Comparison between experimental and predicted molar fractions (dry basis) of (a) CO and (b) NO in the flue gases for different thermal loads.

morphology. In particular, some flames issuing from the holes also merge as we can observe from the thermal field in Fig. 8a. This behavior reflects the fact that some holes are more fed than others by the distributor, as preliminary shown in Fig. 4. The interaction between neighbor flames is even more evident in the region of the slits, where a complex flame structure is present: we observe that the flames issuing from a group of four slits merge into a single intense flame. Not all flames are equal, reflecting the fact that the slits are fed with different flow rates from the distributor. Furthermore, there are extinguishing zones in the extreme regions of the burner, as we can see in the plane crossing the slits (Fig. 8b). This phenomenon is well in agreement with the experimental tests carried out in open air shown in Fig. 7b.

Fig. 10 shows the thermal field in the heat exchanger region for the minimum and nominal load. The flow field is also shown through black vectors. We can observe how the flue gas crosses the heat exchanger region toward the outlet.

A good prediction of the flue gas cooling is essential for an accurate estimation of the emission of carbon monoxide, as discussed and shown in the paper of [32]. The comparison between experimental and predicted CO emissions is provided in Fig. 11a. We observe that the agreement is very satisfactory for both loads. In particular, the model well estimates the amount of CO of few ppm for the smallest load, while correctly predicts that the CO emissions rise to approximately 120 ÷ 150 ppm for the nominal load. We highlight that the predicted CO emissions are very dependent on the heat exchanger model. Indeed, even though detailed kinetics is used for the flame region, the conjugate heat transfer approach is mandatory as it enables a more realistic prediction of the heat exchanger region. Other treatment of the cooling regions, ads for instance by modeling the coils with uniform wall temperature as boundary condition, lead to erroneous CO estimation.

Nitric oxides are given in Fig. 11b. Again, we observe an excellent prediction of the CFD model, especially by considering that the emissions are of a few ppm. This evidence demonstrates that the thermochemical field is well captured with the detailed kinetics as NO emissions depend strongly on temperature and radicals such as the O radical.

Effect of H_2 content

The impact of hydrogen addition to the gas mixture on the combustion process in the condensing boiler is analysed by considering H_2 content up to 50% by vol. As described in Section 2, when we add hydrogen to the gas mixture, we observe a decrease of both thermal load and equivalence ratio, as estimated in Table 1. This means that naturally the boiler

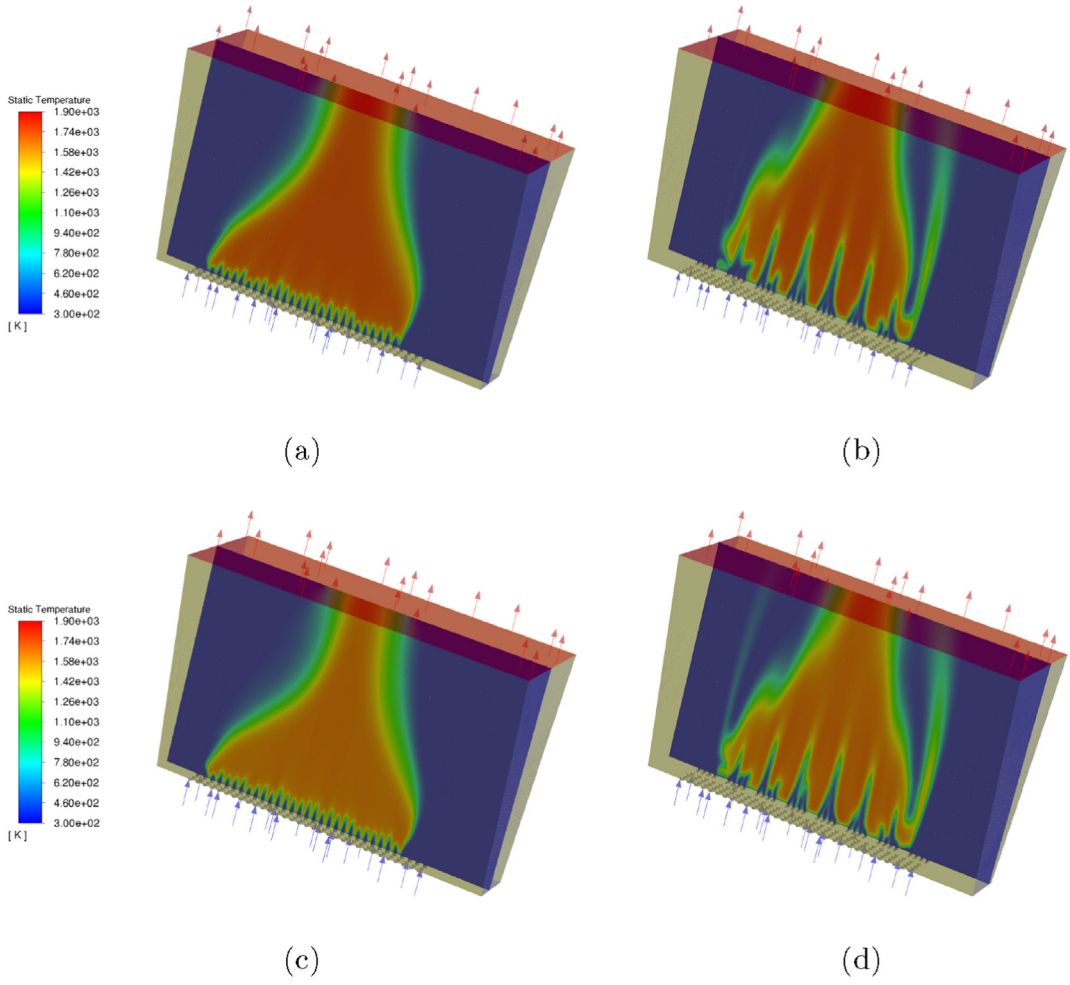

Fig. 12 – Temperature field for a plane passing through a row of +(a, c) holes and (b, d) slits for the nominal power (25 kW) and for: (a,b) G222, (c,d) H2NG test gases.

tends to operate in more dilute conditions, i.e., by withdrawing more excess of air. The thermal field in the burner region is reported in Fig. 12 for the G222 (23% by vol. of hydrogen) and H2NG (50% by vol. of hydrogen) at the nominal load, by showing the same planes crossing the groups of holes and slits as for natural gas (i.e., G20 in Fig. 8). Firstly, we observe how the peak temperature diminishes with increasing the H_2 content from 1970 K with the G20 test gas to 1870 K and 1740 K for the G222 and H2NG mixtures. Indeed, even though we all know that hydrogen gives a higher adiabatic flame temperature than methane, this behavior is well compensated by the higher dilution, that ultimately leads to a reduction of the peak temperatures. The flame morphology can be appreciated by the OH fields, reported in Fig. 13. Here we can see that the high reactivity of hydrogen is hampered by the larger dilution. Indeed the OH levels are weaker than for methane. In particular for methane we observed a strong interaction between flames from neighbor holes (see Fig. 9), while this interaction can hardly be discerned for 23% of H_2 (Figs. 13a) and 50% of H_2 (Fig. 13c). As for the region of the slits, we observe a strong interaction between neighbor flames that merge for all hydrogen contents. In all cases the behavior is similar, with a decrease of the OH peaks and of the flame height with increasing the hydrogen content (please, compare Fig. 8b for G20 to Fig. 12b,d in presence of increasing percentage of H_2).

The impact of hydrogen addition on pollutant emissions is summarized in Fig. 14 which compares measured and predicted emissions for the three investigated gas mixture at 25 kW. Adding hydrogen leads to a reduction of the CO emissions, from 153 ppm (experimental measurement, while 120 ppm is the predicted value) for natural gas to 18 ppm (predicted value is 24 ppm) when feeding 50% by vol. of H_2. Logically, increasing hydrogen, we have a decrease of the available carbon; moreover the thermal load also decreases favoring lower CO emissions. As for NO, we observe that the addition of hydrogen leads to a significant decrease in the emissions, the measurements indicating a reduction from 20 ppm for natural gas to 5 ppm with 50% of H_2. This is an important result, as one of the major concerns in using

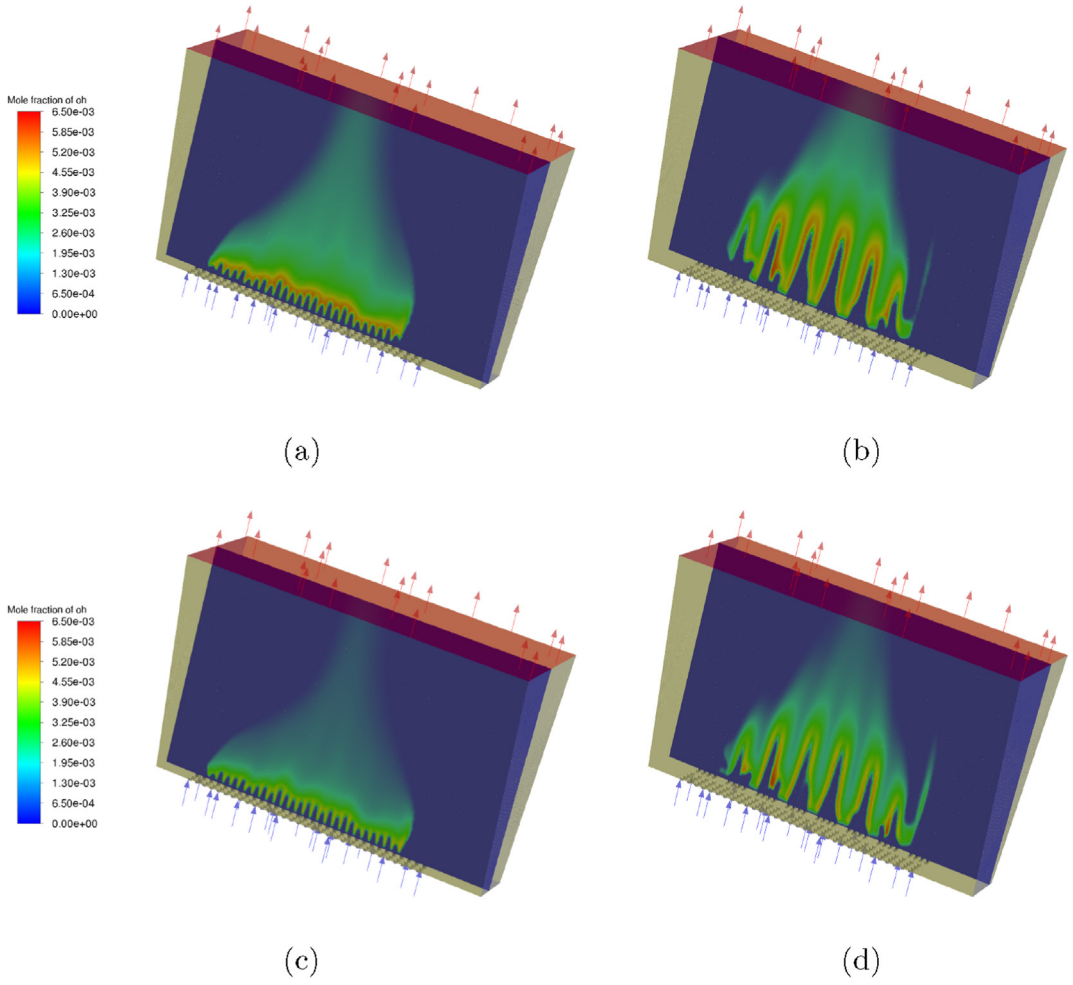

Fig. 13 – OH field for a plane passing through a row of (a, c) holes and (b, d) slits for the nominal power (25 kW) and for: (a,b) G222, (c,d) H2NG test gases.

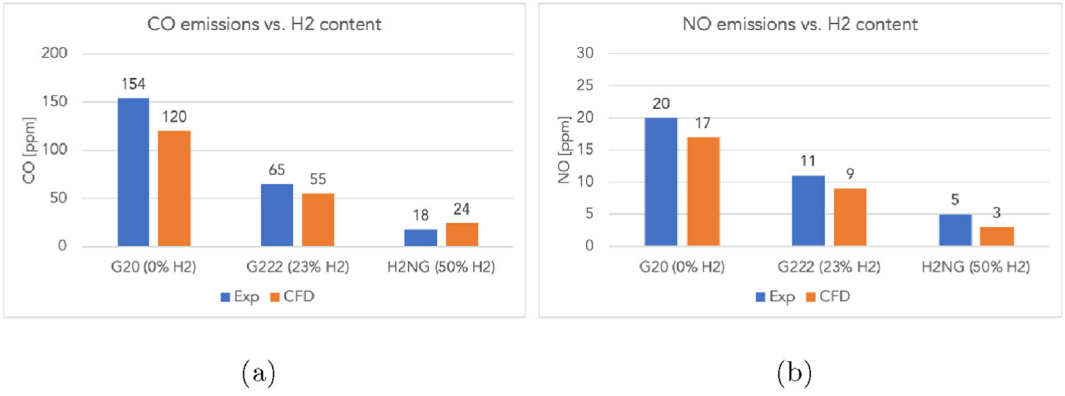

Fig. 14 – Comparison between experimental and predicted molar fractions (dry basis) of (a) CO and (b) NO in the flue gases for different H_2 contents at the nominal power (25 kW).

hydrogen is the high adiabatic flame temperature that may boost the production of NO emissions via the thermal route. Here, we observe exactly the opposite. Indeed, the domestic boiler naturally adjusts itself towards more dilute conditions, which limit the temperature peaks (as observed in the thermal fields of Figs. 9 and 13). As a result, the thermal NO formation is hampered. The presence of H_2 favors other NO formation routes, such as the NNH one [29], taken into account in the present work; however, this formation path does not prevail over the reduction of the thermal route. As for the prediction,

we observe an excellent agreement with the measurements for all H_2 contents, indicating can correctly predict the combustion process, including the production of pollutants.

Conclusions

A numerical model based on CFD with detailed kinetic is used to estimate the impact of adding hydrogen to the gas mixture fed into a condensing boiler equipped with a perforated burner. Importantly, the model has to include the flow distributor, located upstream of the burner as it influences strongly the flow velocity at each hole and slit. This velocity has a direct impact on the flame morphology. Indeed, in the high-velocity region, we observe a strong interaction of flames issuing from neighbor holes or slits. Indeed, while for low velocities and thermal load the flames from groups of holes appear separated, for the high velocity typical of the nominal power, we see some flames merging from neighbor holes. This behavior always occurs for the slits, where a group of 4 slits generates a single intense flame. The general behavior of the combustion chamber does not change with adding hydrogen, even though the peak temperatures decrease and the flames are less intense, as proved by the distribution of the OH radicals. The reason for this behavior is that when with add hydrogen, the boiler naturally withdraws a higher amount of air that dilutes the flames.

The CFD model ensures very good predictions of the NO emissions for all investigated power and hydrogen concentrations, indicating that in all cases the accuracy of the thermal and concentration fields. Indeed, NO depends strongly on both temperature and chemical species (including radicals) which are transported when using detailed kinetics. Indeed, this level of agreement cannot be achieved with global kinetics. Emissions of nitric oxides diminish with the thermal load but also with hydrogen. This is a surprising result that is opposite to the common opinion that the use of hydrogen leads to a higher production of NO. The reason for this positive effect is due to the natural increased dilution which mitigates the thermal formation of NO. Indeed, although hydrogen may promote formation of NO via the NNH intermediate, the thermal route still is the predominant pathway [29] at least up to the maximum H_2 content considered here. Hence, the introduction of green hydrogen has a beneficial effect non only on the CO_2 reduction, but also on the emissions of nitric oxides.

As for CO emissions, also in this case predictions match closely the experimental measurements, which indicate a reduction of CO with increasing the H_2 content. This agreement is possible only when treating accurately the heat exchanger, which is effectively included in the domain by adopting the conjugate heat transfer approach. Indeed, as well discussed in Ref. [32] the accurate prediction of the flue gas cooling is needed to capture the CO emissions.

We believe the present model may provide a practical tool to investigate the effect of feeding some amount of green energy vectors to domestic condensing boilers to help the ecological transition of the residential sector. The model may be used to devise strategies to improve combustion and limit emissions, also by paying attention to the distributor and burner zone. Indeed combustion is domestic boiler has not been an issue so far, with the burner design being manly driven by trial-and-error procedures. The availability of reliable numerical model offers us the opportunity to understand and comprehend the combustion physics inside the boiler and this comprehension is highly needed to effectively implement low-carbon solutions in condensing boilers.

Author contributions

Rachele Lamioni: Conceptualization, Methodology, Data curation, Writing-Original draft preparation. Cristiana Bronzoni, Marco Folli and Leonardo Tognotti: Reviewing and Editing. Chiara Galletti: Conceptualization, Methodology, Writing-Original draft preparation.

Declaration of competing interest

The authors declare that they have no known competing financial interests or personal relationships that could have appeared to influence the work reported in this paper.

Acknowledgments

The present work was supported by the POR FESR 2014–2020 “HyPOWERED” project, funded by Regione Emilia-Romagna Italy. The authors thank Polidoro S.p.A. (Italy) for sharing with us the images of the burner and Condevo S.p.A. for providing us with the coil information.

Appendix A. Supplementary data

Supplementary data to this article can be found online at https://doi.org/10.1016/j.ijhydene.2023.02.040.

REFERENCES

[1] EU Commission Press Release European Green Deal. The Commission proposes transformation of EU economy and society to meet climate ambitions. 14 July. 2021. https://ec.europa.eu/commission/presscorner/detail/en/IP_21_354.
[2] REPowerEU. A plan to rapidly reduce dependence on Russian fossil fuels and fast forward the green transition. 18 May. 2022. https://ec.europa.eu/commission/presscorner/detail/en/IP_22_3131.
[3] Cavana M, Mazza A, Chicco G, Leone P. Electrical and gas networks coupling through hydrogen blending under increasing distributed photovoltaic generation. Appl Energy 2021;290:116764. https://doi.org/10.1016/j.apenergy.2021.116764.
[4] Quarton CJ, Samsatli S. Should we inject hydrogen into gas grids? Practicalities and whole-system value chain optimisation. Appl Energy 2020;275:115–72. https://doi.org/10.1016/j.apenergy.2020.115172.
[5] Olympios AV, Aunedi M, Mersch M, Krishnaswamy A, Stollery C, Pantaleo AM, Sapin P, Strbac G, Markides CN.

Delivering net-zero carbon heat: technoeconomic and whole-system comparisons of domestic electricity- and hydrogen-driven technologies in the UK. Energy Convers Manag 2022;262:115649. https://doi.org/10.1016/j.enconman.2022.115649.
[6] Mouli-Castillo J, Orr G, Thomas J, Hardy N, Crowther M, Haszeldine RS, Wheeldon M, McIntosh A. A comparative study of odorants for gas escape detection of natural gas and hydrogen. Int J Hydrogen Energy 2021;46(27):14881–93. https://doi.org/10.1016/j.ijhydene.2021.01.211.
[7] Dawood F, Anda M, Shafiullah G. Hydrogen production for energy: an overview. Int J Hydrogen Energy 2020;45(7):3847–69. https://doi.org/10.1016/j.ijhydene.2019.12.059.
[8] Gahleitner G. Hydrogen from renewable electricity: an international review of power-to-gas pilot plants for stationary applications. Int J Hydrogen Energy 2013;38(5):2039–61. https://doi.org/10.1016/j.ijhydene.2012.12.010.
[9] McKenna R, Bchini Q, Weinand J, Michaelis J, König S, Köppel W, Fichtner W. The future role of power-to-gas in the energy transition: regional and local techno-economic analyses in baden-württemberg. Appl Energy 2018;212:386–400. https://doi.org/10.1016/j.apenergy.2017.12.017.
[10] Michalski J, Bünger U, Crotogino F, Donadei S, Schneider G-S, Pregger T, Cao K-K, Heide D. Hydrogen generation by electrolysis and storage in salt caverns: potentials, economics and systems aspects with regard to the German energy transition. Int J Hydrogen Energy 2017;42(19):13427–43. https://doi.org/10.1016/j.ijhydene.2017.02.102.
[11] Kovač A, Paranos M, Marciuš D. Hydrogen in energy transition: a review. Int J Hydrogen Energy 2021;46(16):10016–35. https://doi.org/10.1016/j.ijhydene.2020.11.256.
[12] Aniello A, Poinsot T, Selle L, Schuller T. Hydrogen substitution of natural-gas in premixed burners and implications for blow-off and flashback limits. Int J Hydrogen Energy 2022;47(77):33067–81. https://doi.org/10.1016/j.ijhydene.2022.07.066.
[13] Kıymaz TB, Böncü E, Güleryüz D, Karaca M, Yılmaz B, Allouis C, Gökalp İskender. Numerical investigations on flashback dynamics of premixed methane-hydrogen-air laminar flames. Int J Hydrogen Energy 2022;47(59):25022–33. https://doi.org/10.1016/j.ijhydene.2022.05.230.
[14] Zhao Y, McDonell V, Samuelsen S. Influence of hydrogen addition to pipeline natural gas on the combustion performance of a cooktop burner. Int J Hydrogen Energy 2019;44(23):12239–53. https://doi.org/10.1016/j.ijhydene.2019.03.100.
[15] Choudhury S, McDonell VG, Samuelsen S. Combustion performance of low-NOx and conventional storage water heaters operated on hydrogen enriched natural gas. Int J Hydrogen Energy 2020;45(3):2405–17. https://doi.org/10.1016/j.ijhydene.2019.11.043.
[16] Pers H, Aniello A, Morisseau F, Schuller T. Autoignition-induced flashback in hydrogen-enriched laminar premixed burners. Int J Hydrogen Energy 2022. https://doi.org/10.1016/j.ijhydene.2022.12.041.
[17] Boulahlib M, Medaerts F, Boukhalfa M. Experimental study of a domestic boiler using hydrogen methane blend and fuel-rich staged combustion. Int J Hydrogen Energy 2021;46(75):37628–40. https://doi.org/10.1016/j.ijhydene.2021.01.103. international Symposium on Sustainable Hydrogen 2019.
[18] Hodges J, Geary W, Graham S, Hooker P, Goff R. Injecting hydrogen into the gas network-a literature search. URL. 2015. https://www.hse.gov.uk/research/rrpdf/rr1047.pdf.
[19] Smith C, Mouli-Castillo J, van der Horst D, Haszeldine S, Lane M. Towards a 100% hydrogen domestic gas network: regulatory and commercial barriers to the first demonstrator project in the United Kingdom. Int J Hydrogen Energy 2022;47(55):23071–83. https://doi.org/10.1016/j.ijhydene.2022.05.123.
[20] de Vries H, Levinsky HB. Flashback, burning velocities and hydrogen admixture: domestic appliance approval, gas regulation and appliance development. Appl Energy 2020;259:114116. https://doi.org/10.1016/j.apenergy.2019.114116.
[21] Schiro F, Stoppato A. Experimental investigation of emissions and flame stability for steel and metal fiber cylindrical premixed burners. Combust Sci Technol 2019;191(3):453–71. https://doi.org/10.1080/00102202.2018.1500556.
[22] Halter F, Chauveau C, Gökalp I. Characterization of the effects of hydrogen addition in premixed methane/air flames. Int J Hydrogen Energy 2007;32(13):2585–92. https://doi.org/10.1016/j.ijhydene.2006.11.033. iCHS-2005.
[23] Zhao DF, Liu FG, You XY, Zhang R, Zhang BL, He GL. Optimization of a premixed cylindrical burner for low pollutant emission. Energy Convers Manag 2015;99:151–60.
[24] Zhang TH, Liu FG, You XY. Optimization of gas mixing system of premixed burner based on CFD analysis. Energy Convers Manag 2014;85:131–9. https://doi.org/10.1016/J.ENCONMAN.2014.05.055.
[25] H. Altay, S. Park, D. Wu, D. Wee, A. Annaswamy, A. Ghoniem, Modeling the dynamic response of a laminar perforated-plate stabilized flame, Proc Combust Inst (1) 1359–1366. doi:10.1016/J.PROCI.2008.06.099.
[26] Kedia KS, Ghoniem AF. Mechanisms of stabilization and blowoff of a premixed flame downstream of a heat-conducting perforated plate. Combust Flame 2012;159(3):1055–69. https://doi.org/10.1016/j.combustflame.2011.10.014.
[27] Jithin EV, Kishore VR, Varghese RJ. Three-dimensional simulations of steady perforated-plate stabilized propane-air premixed flames. Energy Fuel 2014;28(8):5415–25. https://doi.org/10.1021/ef401903y.
[28] Valiev DM, Akkerman V, Kuznetsov M, Eriksson L-E, Law CK, Bychkov V. Influence of gas compression on flame acceleration in the early stage of burning in tubes. Combust Flame 2013;160(1):97–111. https://doi.org/10.1016/j.combustflame.2012.09.002.
[29] Lamioni R, Bronzoni C, Folli M, Tognotti L, Galletti C. Feeding H_2-admixtures to domestic condensing boilers: numerical simulations of combustion and pollutant formation in multi-hole burners. Appl Energy 2022;309:118379. https://doi.org/10.1016/j.apenergy.2021.118379.
[30] Lamioni R, Bronzoni C, Folli M, Tognotti L, Galletti C. Effect of slit pattern on the structure of premixed flames issuing from perforated burners in domestic condensing boilers. Combust Theor Model 2022:1–26. https://doi.org/10.1080/13647830.2022.2157753.
[31] Hassan G, Pourkashanian M, Ingham D, Ma L, Taylor S. Reduction in pollutants emissions from domestic boilers - computational fluid dynamics study. J Therm Sci Eng Appl 2009;1(1).
[32] Hinrichs J, Felsmann D, Schweitzer-De Bortoli S, Tomczak H-J, Pitsch H. Numerical and experimental investigation of pollutant formation and emissions in a full-scale cylindrical heating unit of a condensing gas boiler. Appl Energy 2018;229:977–89.
[33] Hinrichs J, Schweitzer-De Bortoli S, Pitsch H. 3D modeling framework and investigation of pollutant formation in a condensing gas boiler. Fuel 2021;300:120916. https://doi.org/10.1016/j.fuel.2021.120916.

[34] Polidoro, S.p.A.. https://www.polidoro.com/product/steel-premix.
[35] Condevo S.p.A. https://www.condevo.com/.
[36] Soltanian H, Targhi MZ, Pasdarshahri H. Chemiluminescence usage in finding optimum operating range of multi-hole burners. Energy 2019;180:398–404. https://doi.org/10.1016/j.energy.2019.05.104.
[37] de Vries H, Mokhov AV, Levinsky HB. The impact of natural gas/hydrogen mixtures on the performance of end-use equipment: interchangeability analysis for domestic appliances. Appl Energy 2017;208:1007–19.
[38] Goodwin DG, Speth RL, Moffat HK, Weber BW. Cantera: an object-oriented software toolkit for chemical kinetics, thermodynamics, and transport processes. doi:10.5281/zenodo.4527812. 2021. https://www.cantera.org.
[39] Bilger R, Stårner S, Kee R. On reduced mechanisms for methane-air combustion in nonpremixed flames. Combust Flame 1990;80(2):135–49. https://doi.org/10.1016/0010-2180(90)90122-8.
[40] Cheng P. Two-dimensional radiating gas flow by a moment method. AIAA J 1964;2(9):1662–4.
[41] Siegel R, Howell JR. Thermal radiation heat transfer. Washington DC: hemisphere pub, Corp.; 1992.
[42] Smith T, Shen Z, Friedman J. Evaluation of coefficients for the weighted sum of gray gases model. 1982.
[43] Ansys, Fluent. 19.2 user's guide. Ansys Inc; 2019.
[44] De Soete G. Overall reaction rates of NO and N_2 formation from fuel nitrogen. Symposium (International) on Combustion 1975;15(1):1093–102. https://doi.org/10.1016/S0082-0784(75)80374-2. fifteenth Symposium (International) on Combustion.
[45] Malte P, Pratt D. Measurement of atomic oxygen and nitrogen oxides in jet-stirred combustion. 15th Symposium (International) on Combustion 1975;15(1):1061–70. https://doi.org/10.1016/S0082-0784(75)80371-7.
[46] Konnov A, Colson G, De Ruyck J. NO formation rates for hydrogen combustion in stirred reactors. Fuel 2001;80(1):49–65. https://doi.org/10.1016/S0016-2361(00)00060-0.
[47] Galletti C, Parente A, Derudi M, Rota R, Tognotti L. Numerical and experimental analysis of NO emissions from a lab-scale burner fed with hydrogen-enriched fuels and operating in MILD combustion. Int J Hydrogen Energy 2009;34(19):8339–51. https://doi.org/10.1016/j.ijhydene.2009.07.095.
[48] Parente A, Galletti C, Tognotti L. A simplified approach for predicting NO formation in MILD combustion of CH_4–H_2 mixtures. Proc Combust Inst 2011;33(2):3343–50. https://doi.org/10.1016/j.proci.2010.06.141.